IOP Publishing and International Atomic Energy Agency Nuclear Fusion
Nucl. Fusion **47** (2007) 943–951 doi:10.1088/0029-5515/47/8/028

Development of ITER-relevant plasma control solutions at DIII-D

D.A. Humphreys[1], J.R. Ferron[1], M. Bakhtiari[2], J.A. Blair[3], Y. In[4], G.L. Jackson[1], H. Jhang[5], R.D. Johnson[1], J.S. Kim[4], R.J. LaHaye[1], J.A. Leuer[1], B.G. Penaflor[1], E. Schuster[3], M.L. Walker[1], H. Wang[6], A.S. Welander[1] and D.G. Whyte[2]

[1] General Atomics, PO Box 85608, San Diego, CA 92186-5608, USA
[2] University of Wisconsin, Madison, WI, USA
[3] Lehigh University, Bethlehem, PA, USA
[4] Far-Tech, Inc., San Diego, CA, USA
[5] NFRC/KSTAR, Daejon, Korea
[6] ASIPP/EAST, Hefei, People's Republic of China

Received 29 January 2007, accepted for publication 5 May 2007
Published 24 July 2007
Online at stacks.iop.org/NF/47/943

Abstract
The requirements of the DIII-D physics program have led to the development of many operational control results with direct relevance to ITER. These include new algorithms for robust and sustained stabilization of neoclassical tearing modes with electron cyclotron current drive, model-based controllers for stabilization of the resistive wall mode in the presence of ELMs, coupled linear–nonlinear algorithms to provide good dynamic axisymmetric control while avoiding coil current limits, and adaptation of the DIII-D plasma control system (PCS) to operate next-generation superconducting tokamaks. Development of integrated plasma control (IPC), a systematic approach to model-based design and controller verification, has enabled successful experimental application of high reliability control algorithms requiring a minimum of machine operations time for testing and tuning. The DIII-D PCS hardware and software and its versions adapted for other devices can be connected to IPC simulations to confirm control function prior to experimental use. This capability has been important in control system implementation for tokamaks under construction and is expected to be critical for ITER.

PACS numbers: 52.55.Fa, 52.65.Kj, 07.05.Dz

1. Introduction

As the first operating burning plasma device, control performance requirements in ITER [1] will exceed those of present-day experiments. In addition, the ability to use operational time to empirically and iteratively improve control performance will be severely constrained by machine protection limits and availability of experimental time. Under these conditions, the need for systematic model-based control design tools is critical. A long-time program of control development has produced many control solutions and an extensive set of modelling and design tools for development of controllers to support the demanding Advanced Tokamak (AT) mission of DIII-D [2]. These control solutions and computational tools provide many of the functions that will be needed for ITER control, design and verification, and complement contributions by other devices with strong focus on plasma control [3–9]. Over the last decade, a computational environment for tokamak modelling and control design originally developed for DIII-D has also been applied to many present and next-generation devices (including ITER) and, in particular, to operating devices that share the DIII-D plasma control system (PCS) [10]. Section 2 describes this highly flexible environment, its application to next-generation devices, and its use in design and verification of control algorithms. New PCS algorithms addressing ITER-relevant control issues including fault detection and response are also described.

DIII-D integrated plasma control (IPC) tools have been successfully applied to design and operational use of improved algorithms for suppression of neoclassical tearing modes (NTMs). Simulations of island dynamics in response to applied electron cyclotron current drive (ECCD) have enabled use of new algorithms (typically successful on first operation of application) including real-time tracking of q-profile evolution to maintain ECCD/island alignment following island suppression [11]. This capability will be required in order to sustain robust suppression of NTMs in ITER which, in

turn, will reduce the likelihood of disruption and increase the attainable plasma beta. Because the present ITER design locates the ECCD launchers at a high outboard poloidal position, current deposition will be broad and its effectiveness in island suppression is expected to be correspondingly lower. In this case, alignment accuracy alone will not be sufficient to fully stabilize the mode. Modulation of gyrotron power to drive current near the O-point while avoiding driving current near the island X-point is expected to be essential as well [12]. Driving current near the island O-point serves to replace missing bootstrap current, while driving current near the X-point can actually destabilize the mode more. The ability to use modulated ECCD in this way to enhance the mode suppression effectiveness depends on having a rotating plasma (and island), and on determining the frequency and phase of that rotating island. New PCS hardware and algorithms have been developed to accomplish the required high frequency modulation and phase alignment to demonstrate this control action in DIII-D. Section 3 describes experimental use of q-profile tracking and development of new gyrotron modulation control in DIII-D.

The ITER poloidal field (PF) coil set is highly optimized to provide sufficient plasma shape flexibility while satisfying cost constraints. This optimization implies a significant amount of operation near coil current limits. Algorithms that can maximize the distance from these limits while maintaining good axisymmetric control will be necessary to enable robust operation of ITER equilibria. While DIII-D is not as tightly constrained as ITER, ever-increasing exploration of its operating space has led to similar operation near coil current limits, necessitating the same type of algorithms. A nonlinear algorithm that accomplishes this same current limit avoidance with minimal detrimental impact on shape control has been developed and demonstrated experimentally on DIII-D. Section 4 outlines the algorithm itself and summarizes results from its experimental application.

ITER is expected to explore the higher beta regimes that should be accessible following stabilization of the resistive wall mode (RWM). Although the algorithms required to produce such stabilization are relatively complex, the experimental time expected to be available in ITER for control optimization will be limited. Thus, controllers must be developed based on validated plasma-conductor models, and both the implementation and the expected performance must be extensively verified with simulations prior to experimental use. As in all applications of IPC, the design must be accomplished primarily using 'control level' models. Such models describe the essential dynamic characteristics of the elements of the control system, while being of sufficiently low order and simplicity to allow rapid analysis and iteration. Section 5 describes such a low order yet accurate dynamic model of the DIII-D RWM system which is readily applicable to next-generation devices. Application of IPC to this model illustrates the design of high robustness controllers and identifies several important characteristics of the RWM problem.

2. Integrated plasma control

IPC is a systematic approach to design and verification of controllers for tokamak operation. The approach is characterized by control designs using physics-based models validated by experimental results, confirmation of performance in the presence of detailed system dynamics (e.g. power supply saturation), and verification of both controller implementation and performance by operating actual control software and hardware against simulations. Use of validated physics-based models is essential in order to allow high confidence extrapolation to related regimes in devices which do not yet exist or which have not produced those regimes. System-identified or database-trained models, for example, are difficult or impossible to extrapolate with confidence.

The IPC approach is realized by the TokSys modelling and simulation environment, developed at DIII-D and now applied to and in use on many devices worldwide. This environment, implemented in Matlab® and Simulink® (http://www.mathworks.com), includes tools for construction of axisymmetric and nonaxisymmetric MHD control models in tokamaks, for design of relevant controllers, and for testing against nonlinear simulations. Figure 1 illustrates the process of model definition in the TokSys environment, and summarizes elements embodying the IPC approach. Moving from top to bottom and left to right, the figure shows elements included in construction of axisymmetric models (top/left) and nonaxisymmetric models (bottom/left) which are very similar in many ways. Both categories of model require specification of data describing the geometries, material properties, and general system descriptions. These data are typically supplied by a given project in their own choice of units and listing format. These are converted to a standard format used throughout TokSys, and are passed to a set of vacuum calculation modules. These calculations predominantly produce resistances and inductances for discretized conductor elements, as well as a large number of Green functions (for example, mapping currents in conductors to resulting fields on a computational grid). The results of the vacuum calculations are passed to modules which calculate plasma responses. These responses include axisymmetric and nonaxisymmetric instabilities, as well as stable plasma behaviour in response to various actuators (such as control coil currents or applied current drive). Axisymmetric plasma response models calculated by these modules are generally linear, as are RWM models. Models describing the response of NTM magnetic islands are necessarily nonlinear. Integration of vacuum and plasma/actuator models then allows construction of detailed simulations (Simservers), which include nonlinear responses of various actuators (e.g. power supply saturation) and can be connected to the actual PCS for final testing. This verification step (illustrated by the 'Integrated Simserver/simulation-PCS' loop at the far right) is an essential step in the control design process required for a fusion reactor such as ITER. Another key aspect of the TokSys environment is its set of common, generic functions describing fundamental physics responses validated on DIII-D and other devices. Their general structure allows these functions to be directly applied to new tokamak configurations under a common representation.

This generic modelling/simulation environment has been applied to dozens of operating devices, device designs and next-generation devices newly started up or soon to be operating (a partial list includes Alcator C-MOD, FSX, JT-60U, DIII-D, JT-60SC, JT-60SU, SST-1, ITER-LAR,

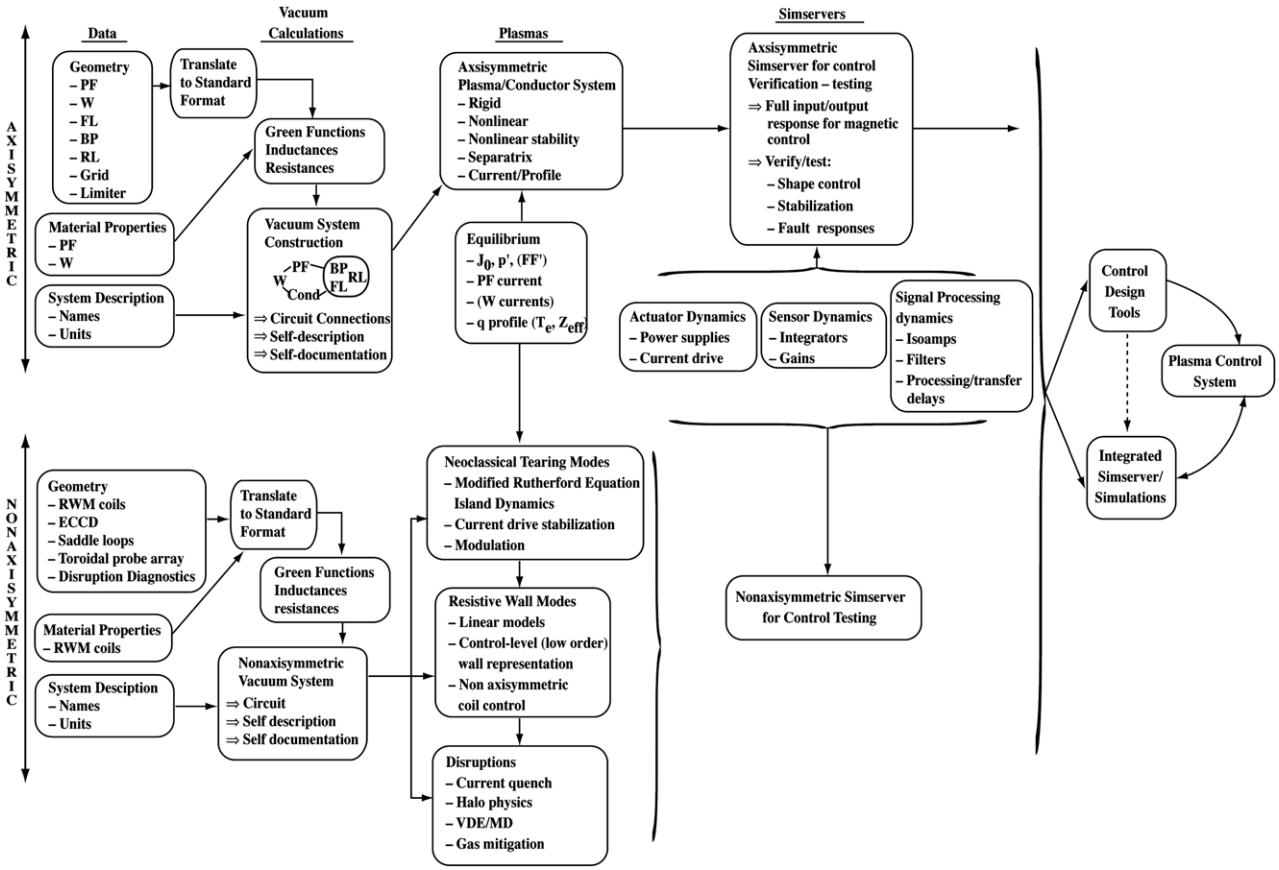

Figure 1. Schematic of the elements of TokSys, a generic modelling and simulation environment in Matlab®/Simulink® that realizes the IPC approach.

ITER-HAR, ITER-FDR, ITER-FEAT, NSTX, Pegasus, KSTAR, EAST, FDF). Figure 2 shows poloidal cross-sections for a selected subset of these devices in the common representation of TokSys. Many of these devices use the DIII-D PCS. The DIII-D PCS is a highly flexible multi-cpu general real-time control environment allowing implementation of arbitrarily complex algorithms. The architecture also enables connection of actual PCS hardware and software to detailed simulations to confirm correct code implementation and control performance prior to experimental use. The generality, flexibility and extensive operational algorithms available in the DIII-D PCS have led to its adoption at fusion experiments worldwide, including MAST [13], NSTX [14], KSTAR [15], EAST [16] and PEGASUS [17]. The combination of the TokSys environment and the PCS has been used to develop and verify startup and shape control algorithms for several of these devices. Many of the features and solutions of the DIII-D PCS satisfy requirements for and can provide useful examples in design of the ITER control system.

One area of DIII-D PCS algorithm development of relevance to ITER is fault response and machine protection, including protection of superconducting coils from approaching or exceeding operational limits. A general architecture for flexible fault response has been developed and implemented in the DIII-D and EAST PCS versions. Fault response mechanisms in the EAST PCS detect and respond to overcurrents, large control error signals, or power supply faults. The general architecture allows switching of control phases to a predefined fault response sequence, including flexible access to any control action available to the PCS. For example, gas valves can be closed in response to a fault, or perhaps fully opened in order to trigger a density limit disruption. Power supply voltages can be set to zero, allowing currents to decay away on the resistive L/R time set by the bus/lead resistance. Plasma current can be ramped to zero, and plasma shape can be controlled to lower elongation or returned to a limited configuration. The standard shutdown scenario developed for the EAST PCS includes a phase sequence that will set all power supplies to zero in the case that the fault response results from a faulty current measurement. If the algorithm tried to zero a given coil current in the presence of such a faulty current signal, it is possible that the power supply would accidentally force the current to a large nonzero value instead of zero.

3. Enhanced effectiveness in NTM suppression using q-surface tracking and modulated ECCD

NTM control in DIII-D has benefited from application of the IPC design approach, which has produced several search algorithms to find optimal q-surface/ECCD alignment, as well as active tracking algorithms to maintain alignment of the relevant resonant surface with the ECCD deposition spot after mode stabilization [18]. Recent experiments in

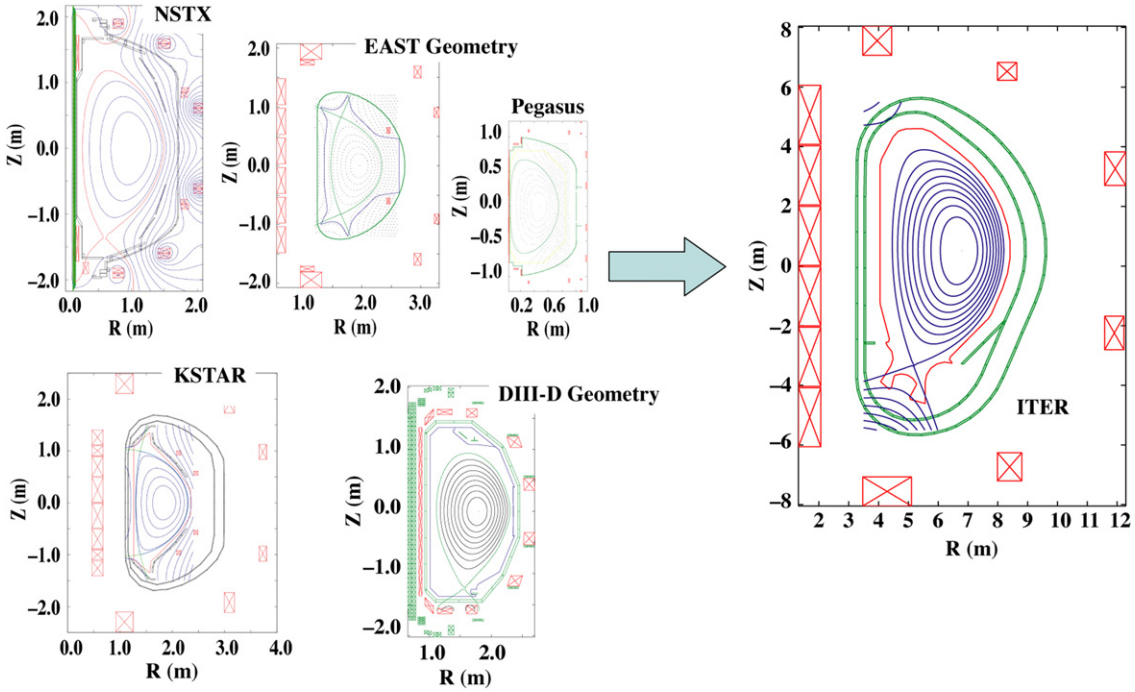

Figure 2. Operating experimental devices and device designs for which TokSys models have been developed and integrated with a version of the DIII-D PCS.

the last two years have demonstrated robust and sustained suppression of the 3/2 and 2/1 NTM (separately) using these algorithms [19]. Active tracking is now accomplished with real-time reconstruction of resonant q-surface geometry using motional Stark effect (MSE) measurements [20]. The Search and Suppress algorithm performs systematic searches in ECCD/island alignment and freezes the alignment when the mode suppression rate is sufficient or when the island is sufficiently suppressed. The plasma major radius can be varied to move the NTM island relative to the nominally fixed deposition location, or the toroidal field can be varied to move the second harmonic resonance relative to the nominally fixed island location. It should be noted that movement of the plasma major radius or toroidal field are presently the only ways available in DIII-D to accomplish the ECCD/island alignment, prior to installation of a real-time-steerable launcher presently planned for 2008. However, because of the way the algorithm is designed, the general control response is readily extensible to this type of actuator without changing the fundamental logic, making the DIII-D Search and Suppress and Active Tracking control approaches readily transferable to ITER.

Figure 3 shows results of an experiment illustrating use of a systematic search algorithm followed by active tracking with real-time q-profile reconstruction. The equilibrium reconstruction shown in figure 3(a) shows a rendering of the 2/1 NTM islands that grow in this discharge prior to $t = 4500$ ms. A rectangular region containing the current deposition spot is outlined in white near the $q = 2$ resonant surface. This rectangular region is expanded in figure 3(b), showing the centre and boundaries of the saturated island, as well as the current deposition spot. Note that the edge of the spot, denoting the full width at half maximum of the current deposition profile, is approximately the half-width of

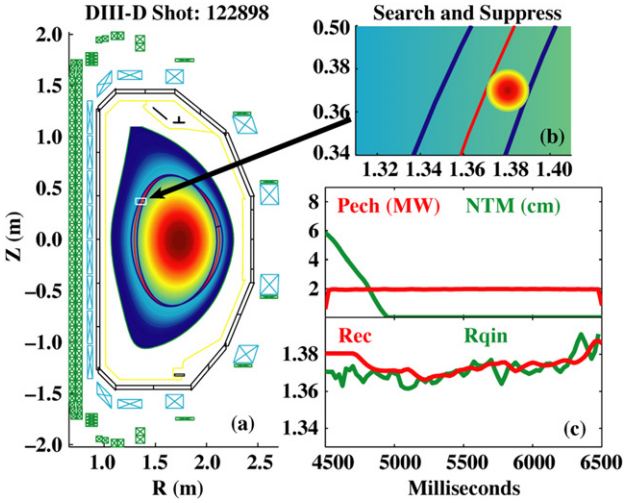

Figure 3. Summary of an experiment illustrating use of the DIII-D Search and Suppress algorithm for NTM stabilization, followed by active tracking with real-time q-profile reconstruction. (a) The equilibrium shows 2/1 NTM island geometry, and (b) the current deposition region is expanded. (c) Time traces show ECH power (Pech) in red, width of the NTM islands in green, major radius of the EC current deposition point (Rec) in red, and major radius of the $q = 2$ surface in green.

the saturated island itself in this region. The gyrotrons are enabled at $t = 4500$ ms (ECH power denoted by 'Pech'), and the island begins to shrink (island width denoted by 'NTM'). Initially the island location ('Rqin') is misaligned with the ECCD ('Rec') by ~1 cm, but the search process moves the plasma major radius to bring them into alignment. Real-time reconstruction of the resonant q-surface allows this alignment to be maintained with 'active tracking' even after the island is

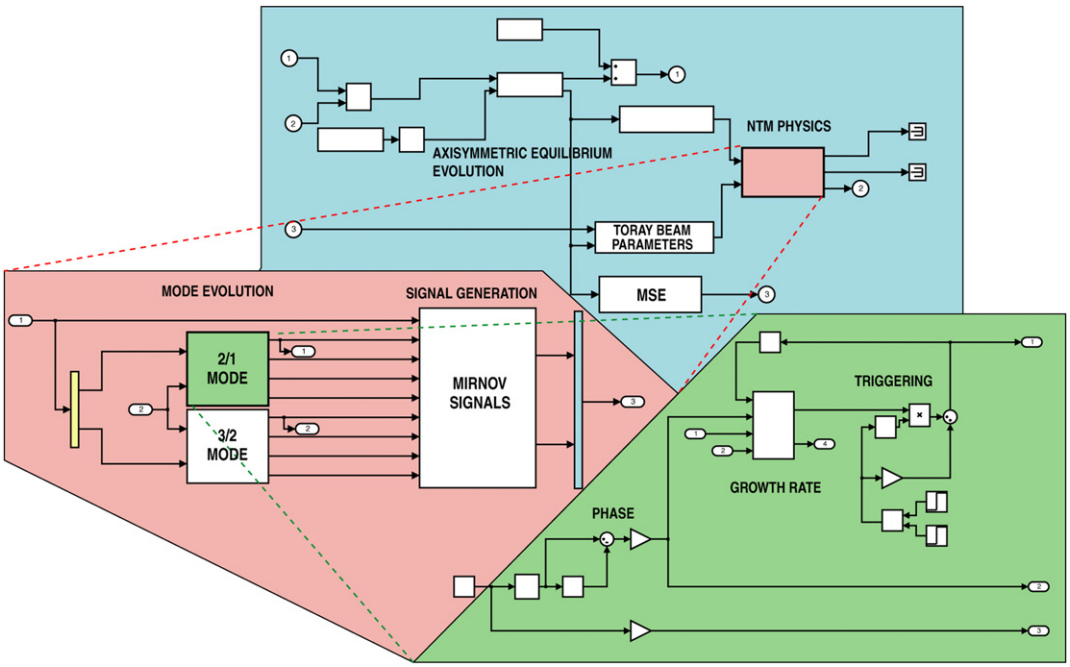

Figure 4. Schematic of the TokSys NTM model for development and verification of NTM suppression control algorithms, showing upgraded elements for gyrotron modulation to enhance efficiency of island stabilization. The model includes modules describing the evolution of the axisymmetric equilibrium (top left), and the evolution of the NTM islands in the presence of applied ECCD (green blocks and green region at bottom right).

suppressed, sustaining the suppression through the end of the control phase.

The active tracking algorithm has also been used to achieve pre-emptive avoidance of the NTM, applying ECCD to the resonant surface prior to raising the plasma beta. As the beta was raised beyond the value which would trigger the mode in the absence of active suppression, the pre-emptive ECCD application prevented the appearance of the mode [21]. Variations in the plasma density can change the refraction of the microwave path and with it the location of the current deposition. The active tracking algorithm has, therefore, been extended to correct for this refraction change based on real-time measurements of the density profile from two interferometer chords [22]. The higher density typical of ITER operation will make this refraction effect more pronounced and will routinely require correction.

The ITER gyrotron launcher port is presently located at a high poloidal angle on the outboard side, producing a broad ECCD deposition footprint. Because the total power available is marginal for the NTM suppression mission [12,23] the current drive must be extremely efficient. One way to maximize suppression efficiency is to modulate the gyrotron signal so as to drive current near the island O-point, and turn off the power when the rotating island X-point passes through the deposition spot. This requires nonzero plasma rotation, as well as the ability to detect the island frequency and phase, and to modulate the gyrotrons at relevant frequencies with specified phase. The DIII-D PCS and gyrotron control system have been upgraded to accomplish this detection and allow modulation of gyrotron power in order to demonstrate this approach. The detection algorithm assumes signals of the form $s_k(t) = A_1 \exp\{\mathrm{i}[\phi_1(t) + \alpha_k]\} + A_2 \exp\{\mathrm{i}\,[\phi_2(t) + 2\alpha_k]\}$ in each probe of a midplane-outboard toroidal array, where α_k is toroidal angle of the probe and ϕ_1, ϕ_2 are the (frequency-dependent, time-varying) phases of the $n = 1$ and $n = 2$ modes. Combining signals leads to a matrix equation $Pa = s$, where $a = [A_{1c}(t) \quad A_{1s}(t) \quad A_{2c}(t) \quad A_{2s}(t)\ ]^{\mathrm{T}}$ is the set of cosine and sine coefficients and $s = [s_1 \quad s_2 \cdots s_9\ ]^{\mathrm{T}}$. A least squares fit to the signal model at each time t is found by solving for a using the pseudoinverse of P. The gyrotrons on DIII–D can be modulated at a maximum of 5 kHz with good waveform shaping. It is undesirable to reduce the rotation much below this level using the new counter-NBI rotation control capability of DIII-D since such low rotation rates will likely lead to locked modes. Since the PCS is unable to generate a high-fidelity modulated square wave at such high frequencies, a dedicated computer is used to generate the signal. The PCS supplies a frequency and phase signal to this dedicated computer based on reconstruction of the mode frequency and phase.

Improved simulations for development of controllers now include island response models that represent the effect of gyrotron modulation on suppression dynamics. Figure 4 summarizes the elements of the TokSys simulation used to test and optimize NTM control performance, which include an island response model and interaction with the axisymmetric equilibrium. The axisymmetric evolution of the plasma equilibrium is calculated in the upper left blue portion of the figure, and the resulting signals are fed to an NTM physics module, along with current deposition characteristics (as calculated offline by the TORAY-GA code). Details of the NTM physics module (pink rectangle) are shown in the pink region shown at the left side of the figure. This module produces the magnetic Mirnov signals resulting from a selectable 2/1 or 3/2 NTM island under the conditions produced by the equilibrium conditions and current deposition. Details of the green block representing the 2/1 mode evolution

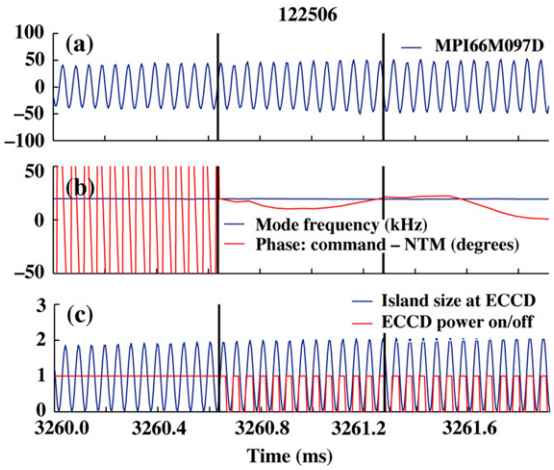

Figure 5. Simulation based on experimental NTM data illustrating island frequency and phase detection for gyrotron modulation in the DIII-D PCS. (*a*) Experimentally measured signal in a single poloidal magnetic field probe on the outboard midplane, part of the array of 11 midplane probes used to reconstruct the island size and phase; (*b*) corresponding detected frequency and phase of the 2/1 island present in this discharge; (*c*) resulting signal to command the power generated by the dedicated gyrotron modulation computer, which is seen to be well-synchronized with the island amplitude.

are shown in the green region at the right side of the figure. The 2/1 and 3/2 mode evolution modules contain representations of the modified Rutherford equation to allow calculation of the mode growth rate. The triggering of the mode (by instabilities that produce seed islands, such as sawteeth or ELMs) is provided in a simple set of nonlinear elements at the output, and the phase of the mode is also separately specified by a set of separate inputs to the mode evolution blocks. Figure 5 shows a simulated control scenario, which is based on actual experimental data in the presence of a 2/1 NTM. Figure 5(*a*) shows the experimentally measured signal in a single poloidal magnetic field probe on the outboard midplane, part of the array of 11 midplane probes used to reconstruct the island size and phase. All of the probes in this array show a clear sinusoidal signal as exemplified by figure 5(*a*), representing the fluctuating field produced by the rotating 2/1 magnetic island. The signals from all of the probes are fitted to $n = 0$, 1, and 2 spatial sinusoids to identify the desired toroidal mode number, and the frequency and phase of these field distributions are extracted from the fit. Figure 5(*b*) shows the corresponding detected frequency and phase of the 2/1 island present in this discharge. When the algorithm is first enabled, an initial period (in this case 640 μs) is required to determine the frequency and phase. This initial period is shown in the first 640 μs of figure 5(*b*). After that initial period, the frequency and phase are updated every 640 μs. Figure 5(*b*) shows the actual time-varying phase of the island (red line), demonstrating that the phase varies slowly enough so that the periodic update is a valid approach. Figure 5(*c*) shows the resulting signal to command the power generated by the dedicated gyrotron modulation computer, which is seen to be well-synchronized with the island amplitude.

The simulation represents a demonstration of the complete control algorithm operating correctly as implemented in the real-time control software. The ability to verify performance and implementation is a key capability of the TokSys integrated control design environment coupled to the DIII-D PCS, and is also an essential requirement of the ITER PCS. Experimental demonstration of modulated gyrotron control in DIII-D is expected in the 2007 operating campaign.

4. Experimental demonstration of nonlinear shape and coil current control algorithms

Good dynamic regulation of the magnetic configuration, including boundary, divertor strikepoints, and location of internal flux surfaces, must be maintained in DIII-D to an accuracy of several millimetres, even in the presence of transient perturbations such as ELMs and sawteeth, over a wide range of shapes and profiles [24]. Axisymmetric control demands in ITER will be challenging, corresponding to shaping and configuration control accuracies (as a fraction of minor radius) comparable to those achieved in DIII-D, but with coils and diagnostics twice as far from the plasma surface (as a fraction of minor radius). Dynamic control constraints will also be greater in ITER than in DIII-D, for example allowing scrapeoff layer contact with the first wall for only brief transients of less than 1 s. Model-based multivariable control design methods allow incorporation of performance requirements in the design process. For DIII-D, such approaches allow designers to trade off aspects of control performance in order to achieve the correct balance required by a given physics experiment. They can also reduce the time spent in tuning control gains in order to allow a discharge to run its programmed duration while avoiding coil current limits. Historically, discharge development in DIII-D has entailed significant adjustment of gains between shots to accomplish this. For ITER, such approaches can provide highly optimized control to make best use of actuators whose capabilities are limited by constraints. In contrast to DIII-D, the ability to minimize or eliminate the need for control tuning is essential to ITER because of the high cost of operations and high subscription of experimental time.

The DIII-D shape control system regulates the flux at various control points located around the plasma boundary to be the same as the flux at the X-point(s) or a selected wall limited point. This 'isoflux' scheme [25] allows high accuracy of boundary control and makes efficient use of the 18 PF coils that surround the DIII-D vessel, conformally to typical plasma shapes. In order to make similarly efficient use of power supply capabilities under this scheme, DIII-D discharges often produce PF current evolutions that approach supply limits. Achieving a given experimental physics goal often requires adjusting isoflux control gains to avoid exceeding these limits. A multivariable model-based controller can allow operators to balance varying experimental control goals without between-shot adjustment, and has been selected as the approach for ITER axisymmetric control. However, such controllers will seek to drive boundary errors to zero, often at the expense of attempting to exceed power supply limits. A nonlinear algorithm is required to prevent this while still maintaining acceptable control performance. Figure 6 shows a DIII-D experimental demonstration of linear model-based multivariable controllers functioning in concert with a nonlinear algorithm to maximize distance from coil current

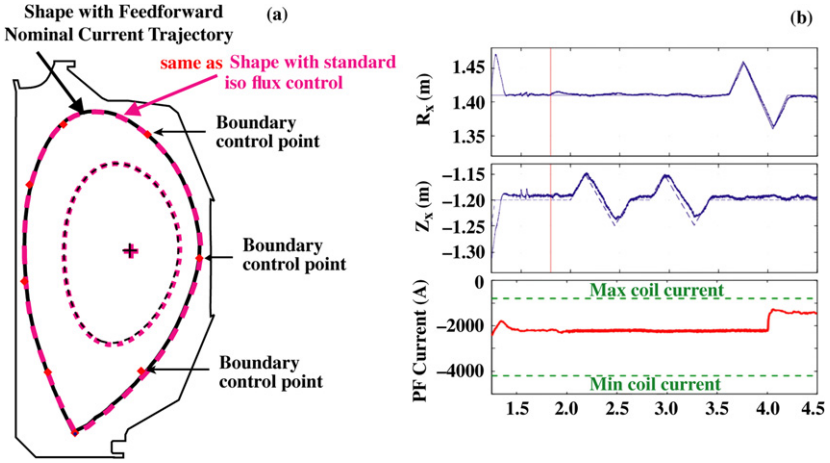

Figure 6. Summary of model-based multivariable boundary control in DIII-D acting in concert with feedforward current trajectories adjusted in real time to maximize distance from coil current limits. (*a*) Comparison of plasma boundaries for isoflux control with (black) and without (red) feedforward current trajectories. (*b*) Experimental time traces showing dynamic control of X-point position (R_x, Z_x), where dashed lines represent target values, solid lines represent experimentally measured values. The bottom frame shows current evolution in a typical PF coil (in which the dashed green lines represent minimum and maximum allowable coil current values).

limits while maintaining good shape and X-point control. The algorithm calculates dynamically varying feedforward current trajectories for all coils, based on a linear plasma response model, in order to balance these competing needs. This approach also provides 'headroom' for coil current excursions in response to transient off-normal events. Figure 6(*a*) compares two equilibria, one under the usual DIII-D shape control without feedforward current trajectories (in which coil currents are produced by shape control action alone), and one with feedforward currents (calculated and produced by the new nonlinear optimization algorithm). The accuracy of control of the plasma boundary is the same in each case. Figure 6(*b*) shows the X-point radial and vertical positions under programmed variation, demonstrating good dynamic control of individual shape quantities with feedforward current trajectories (an example of which is also shown). The PF coil current shown in figure 6(*b*) requires updating by the current trajectory algorithm in the case of the R_x variation, but not for the programmed Z_x change.

Such a linear–nonlinear control system will be essential for ITER in order to provide good control near tightly constrained operating limits throughout a long pulse discharge.

5. RWM control based on finite element eigenmode models

Robustness of RWM stabilization has been observed to be degraded by the effects of ELMs on RWM control response and to be sensitive to the instantaneous growth rate of the mode [26, 27]. New plasma-conductor models have been developed based on an eigenmode representation of the DIII-D passive structure, allowing low-order model-based controllers to be designed.

The model description used in the TokSys RWM modules consists of a first order matrix circuit description:

$$M_{ss}\dot{I}_s + R_{ss}I_s + M_{sp}C_{pp}M_{ps}\dot{I}_s = V_s, \qquad (5.1)$$

where I_s and V_s denote currents and voltages in stabilizing conductors, including both vessel wall and active control coils. C_{pp} is a scalar coupling coefficient between the modal perturbed surface current K_p and the plasma surface flux, ψ_p. Defined by $K_p = C_{pp}\psi_p = C_{pp}(M_{ps}I_s)$, C_{pp} completely describes the effect of the energy source driving the instability. Vessel wall current states can be described by surface current eigenmodes, derived by solving an eigenvalue equation of the form [27]

$$\nabla_s \cdot \left[\frac{\eta}{\Delta}(\vec{\nabla}\nu)^2\,\nabla_s K_m\right] = -(\vec{\nabla}\nu)^2\lambda_m K_m, \qquad (5.2)$$

where $K_m(l,\phi) = \kappa_m(l)\,\mathrm{e}^{-in\phi}$ and the surface Laplacian is given by $\nabla_s = \hat{l}\,(1/R)\,(\partial/\partial l)\,R + \hat{\phi}\,(in/R)$ in the (radial dimension, poloidal length, toroidal angle) coordinate system (ν, l, ϕ). The eigenvalues $\{\lambda_m\}$ play the role of surface resistors with units of resistivity/length^3. The eigensystem (equation (5.2)) is solved and the mutual inductance couplings of equation (5.1) are derived using the finite element representation shown in figure 7.

RWM control in DIII-D is accomplished principally with a set of six picture-frame, in-vessel coils evenly spaced toroidally above the outboard midplane and connected in $n = 1$ pairs, and six identical coils connected in $n = 1$ pairs below the outboard midplane. Although these in-vessel coils (I-coils) have the best coupling to the plasma and least shielding by the vessel wall, a set of ex-vessel coils (C-coils) are also used for low frequency RWM control and error correction. One control approach is to make the control voltages applied to each pair of the set of 12 I-coils depend on estimates of the RWM mode amplitude from magnetic diagnostics. The mode amplitude estimate is performed with a matched filter consisting of the vector of magnetic signals in each diagnostic predicted by a linear MHD stability code [28]. Control studies based on this scheme and the eigenmode model described above have demonstrated that a single choice of control gains can provide good control over a wide range of growth rates, and that high-order multivariable controllers can improve performance over simple proportional–derivative (PD) controllers. Figure 8 shows contours of stability for various mode growth rates using 'diagonal' PD controllers in

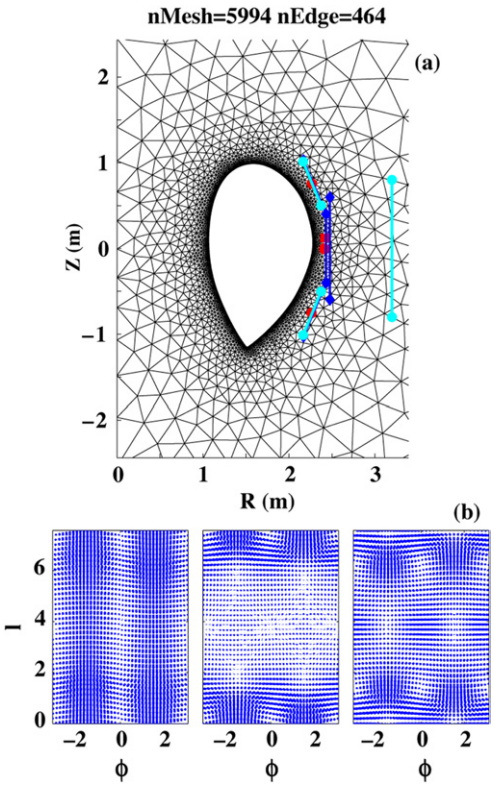

Figure 7. Details of finite element model used to represent the vessel in RWM modelling. (*a*) Mesh representation of DIII-D for calculation of coupling among vessel eigenmodes, active coils, and plasma surface current mode. (*b*) Surface current patterns corresponding to the three eigenmodes with the longest time constants.

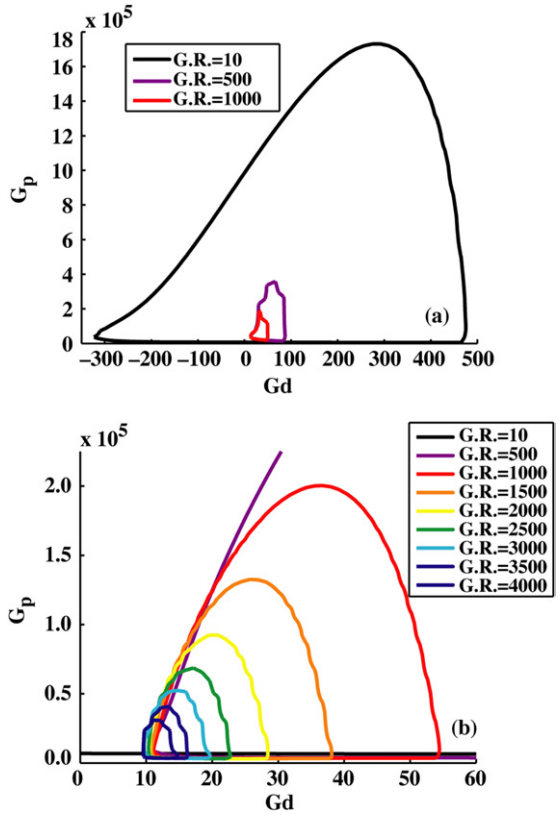

Figure 8. Contours of stable gain spaces for varying RWM growth rates. The interior of each contour corresponds to a closed-loop stabilized RWM. G_p and G_d are the proportional and derivative gains, respectively. GR denotes the growth rate of the mode (in rad s^{-1}) corresponding to each coloured contour. (*a*) Contours defining the closed-loop stable regions for three widely varying choices of growth rate. (*b*) An expansion of the red contour region shown in (*a*), with detailed contours of stable regions corresponding to different open loop RWM growth rates primarily illustrating the range between 1000 and 4000 rad s^{-1}.

this scheme. Such diagonal controllers apply voltage based only on two degrees of freedom corresponding to estimated mode amplitude and phase. Corresponding to these two degrees of freedom, voltages are applied to the coils in two fixed vectors, in such a way as to directly oppose the plasma displacement corresponding to the unstable mode. The space in which the contours are plotted corresponds to the PD gains, G_p and G_d, respectively. Figure 8(*a*) shows that for sufficiently low growth rate (10 rad s^{-1}; black contour) a large stable gain space exists, but the stable region shrinks rapidly as growth rate increases (e.g. 1000 rad s^{-1}; red contour). Figure 8(*b*) magnifies the stable region corresponding to 1000 rad s^{-1}, showing the stable gain spaces continuing to shrink as the growth rate increases to 4000 rad s^{-1}. At a growth rate of ∼4100 rad s^{-1}, the stable space vanishes, and the mode cannot be stabilized beyond this value with such a PD controller. Note that a single pair of PD gains (e.g. $G_p = 20\,000$ and $G_d = 13$) can stabilize this entire range of growth rates, possibly avoiding the need for gain scheduling. Realistic power supply dynamics and the effects of computational delays have been taken into account in this analysis.

In contrast with the PD controller, linear quadratic Gaussian (LQG) controllers have also been designed and analysed. In this case, a single choice of gains are found to allow stabilization of higher growth rates, up to 6200 rad s^{-1}. Unlike the diagonal PD controller, an LQG controller effectively fully populates the gain matrix, and allows broader dynamic range of control response, improving performance over simple PD controllers. This kind of model-based controller has not yet been applied experimentally on DIII-D. However, the corresponding computational algorithms have been implemented in the DIII-D PCS, and simply replace the extensively applied diagonal PID controller algorithm.

6. Summary and conclusions

Owing largely to its superconducting PF coils distant from the plasma surface and the constraints of its burning plasma mission, ITER demands new control algorithms, as well as higher accuracy and more reliable control than required on present-day experiments. The IPC approach, providing a systematic method for designing and confirming high-confidence control algorithms, is particularly important for such a device. Application of DIII-D IPC tools to various areas of specific relevance to ITER control illustrates the power and readiness of this approach to address high performance tokamak control issues from fundamental physics through consequences of detailed implementations. The DIII-D model-based multivariable linear shape and stability control

algorithm coupled with a unique nonlinear feedforward current trajectory algorithm offers a solution to the key ITER problem of operation near coil current limits. Model-based and simulation-verified NTM suppression algorithms using modulated ECCD to maximize current drive effectiveness in DIII-D demonstrate this critical set of capabilities for eventual ITER application. New approaches to RWM system modelling and resulting model-based controllers for DIII-D demonstrate the usefulness of the IPC approach for global MHD mode control, and provide a path to transfer RWM control results from DIII-D to ITER. Model-based RWM controllers for DIII-D based on optimal techniques (LQG) have been found to allow stabilization at higher growth rates than simple PD controllers, and both LQG and PD approaches have enabled stabilization up to the maximum achievable using a single choice of gains (possibly avoiding the need for gain scheduling).

IPC, with broad application on DIII-D and many other devices, provides a path to transfer general control results from present-day experiments to ITER. By emphasizing physics-based models validated on a wide range of operating devices and demonstrating reliable experimental use of the resulting algorithms, control solutions created on any of the devices sharing this common representation and standards of verification can be readily applied to ITER with high confidence in performance.

Acknowledgments

Work supported by US Department of Energy under DE-FC02-04ER54698, DE-FG02-89ER53296, DE-FG02-92ER54141, DE-FG03-99ER82791, DE-FG02-04ER54762.

References

[1] Aymar R., Chuyanov V.A., Huguet M. and Shimomura Y., ITER Joint Central Team and ITER Home Teams 2001 *Nucl. Fusion* **41** 1301
[2] Ferron J.R. *et al* 2002 Progress toward sustained high-performance advanced tokamak discharges in DIII-D *Proc. 29th Plasma Physics and Controlled Fusion Conf. (Montreux, Switzerland, 2002)* (Paris, France: European Physical Society) vol 26B, P1.060
[3] Ariola M., Ambrosino G., Lister J.B., Pironti A., Villone F. and Vyas P. 1999 *Fusion Technol.* **36** 126
[4] Ambrosino G. *et al* and JET-EFDA Contributors 2005 *Fusion Eng. Des.* **74** 521
[5] Joffrin E. *et al* 2006 Physics and operational integrated controls for steady state scenario *Proc. 21st Int. Conf. on Fusion Energy 2006 (Chengdu, 2006)* (Vienna: IAEA) CD-ROM file EX/1-6 and http://www-naweb.iaea.org/napc/physics/FEC/FEC2006/html/index.htm
[6] Yonekawa I., Kawamata Y., Totsuka T., Akasaka H., Sueoka M. and Yoshida H. 2004 *Fusion Eng. Des.* **71** 11
[7] Treutterer W., Zehetbauer T., Mertens V., Neu G., Raupp G., Zasche D. and Asdex Upgrade team 2005 *Fusion Eng. Des.* **74** 501
[8] Stillerman J.A., Ferrara M., Fredian T.W. and Wolfe S.M. 2006 *Fusion Eng. Des.* **81** 1905
[9] Gates D.A. *et al* 2006 *Fusion Eng. Des.* **81** 1911
[10] Penaflor B.G., Ferron J.R., Johnson R.D. and Piglowski D.A. 2004 *Fusion Eng. Des.* **71** 47
[11] Humphreys D.A., Ferron J.R., La Haye R.J., Luce T.C., Petty C.C., Prater R. and Welander A.S. 2006 *Phys. Plasmas* **13** 56113
[12] Lahaye R.J., Prater R., Buttery R.J., Hayashi N., Isayama A., Maraschek M.E., Urso L. and Zohm H. 2006 *Nucl. Fusion* **46** 451
[13] Lloyd B. *et al* 2003 *Nucl. Fusion* **43** 1665
[14] Synakowski E.J. *et al* 2003 *Nucl. Fusion* **43** 1653
[15] Kwon M., Bak J. and Lee G.-S. 2002 *Fusion Sci. Technol.* **42** 167
[16] Wan Y.X., Weng P.D., Li J.G., Yu Q.Q., Gao D.M. and HT-7U TEAM 2003 *Nucl. Fusion* **43** 1279
[17] Garstka *et al* 2006 *Nucl. Fusion* **46** S603
[18] Lahaye R.J. *et al* 2002 *Phys. Plasmas* **9** 2051
[19] Petty C.C., Lahaye R.J., Luce T.C., Humphreys D.A., Hyatt A.W., Prater R., Strait E.J. and Wade M.R. 2004 *Nucl. Fusion* **44** 243
[20] Ferron *et al* 2006 *Nucl. Fusion* **46** L13
[21] Lahaye R.J., Humphreys D.A., Luce T.C., Perkins F.W., Petty C.C., Prater R., Strait E.J. and Welander A.S. 2005 *Nucl. Fusion* **45** L37
[22] Humphreys D.A., Ferron J.R., La Haye R.J., Luce T.C., Petty C.C., Prater R. and Welander A.S. 2006 *Phys. Plasmas* **13** 56113
[23] Saibene G. 2006 *Proc. 21st Int. Conf. on Fusion Energy 2006 (Chengdu, 2006)* (Vienna: IAEA) CD-ROM file IT/P2-14 and http://www-naweb.iaea.org/napc/physics/FEC/FEC2006/html/index.htm
[24] Walker M.L., Humphreys D.A., Johnson R.D. and Leuer J.A. 2005 *Fusion Sci. Technol.* **47** 790
[25] Walker M.L., Humphreys D.A. and Ferron J.R. 1997 Control of plasma poloidal shape and position in the DIII-D tokamak *Proc. 36th IEEE Conf. on Decision and Control (San Diego, CA)* p 3703
[26] Fransson C.M. *et al* 2003 *Phys. Plasmas* **10** 3961
[27] In Y. *et al* 2006 *Phys. Plasmas* **13** 062512
[28] Edgell D.H, Kim J.S., Bogatu I.N., Humphreys D.A. and Turnbull A.D. 2002 *Rev. Sci. Instrum.* **73** 1761